

Title	Nanoscale dynamics and protein adhesivity of alkylamine self-assembled monolayers on graphene
Authors	O'Mahony, Shane;O'Dwyer, Colm;Nijhuis, C. A.;Greer, James C.;Quinn, Aidan J.;Thompson, Damien
Publication date	2013-01-09
Original Citation	O'Mahony, S., O'Dwyer, C., Nijhuis, C. A., Greer, J. C., Quinn, A. J. and Thompson, D. (2013) 'Nanoscale Dynamics and Protein Adhesivity of Alkylamine Self-Assembled Monolayers on Graphene', Langmuir, 29(24), pp. 7271-7282. doi: 10.1021/la304545n
Type of publication	Article (peer-reviewed)
Link to publisher's version	https://pubs.acs.org/doi/10.1021/la304545n - 10.1021/la304545n
Rights	© 2013 American Chemical Society. This document is the Accepted Manuscript version of a Published Work that appeared in final form in Langmuir, copyright © American Chemical Society after peer review and technical editing by the publisher. To access the final edited and published work see https://pubs.acs.org/doi/pdf/10.1021/la304545n
Download date	2025-08-12 20:50:30
Item downloaded from	https://hdl.handle.net/10468/6145



UCC

University College Cork, Ireland
 Coláiste na hOllscoile Corcaigh

Nanoscale dynamics and protein adhesivity of alkylamine self-assembled monolayers on graphene

S. O'Mahony¹, C. O'Dwyer^{2,3}, C.A. Nijhuis^{4,5}, J.C. Greer¹, A.J. Quinn³ and D. Thompson^{1}*

¹Theory Modelling and Design Centre, Tyndall National Institute, University College Cork, Lee Maltings, Dyke Parade, Cork, Ireland. ²Applied Nanoscience Group, Department of Chemistry, University College Cork, Cork, Ireland. ³Micro & Nanoelectronics Centre, Tyndall National Institute, Dyke Parade, University College Cork, Cork, Ireland. ⁴Department of Chemistry, National University of Singapore, 3 Science Drive 3, Singapore 117543. ⁵Graphene Research Centre, National University of Singapore, 2 Science Drive 3, Singapore 117542.

*To whom correspondence should be addressed: damien.thompson@tyndall.ie. Tel: +353-21-490-4063.

Atom-scale molecular dynamics computer simulations are used to probe the structure, dynamics and energetics of alkylamine self-assembled monolayer (SAM) films on graphene, and to model the formation of molecular bilayers and protein complexes on the films. Routes toward the development and exploitation of functionalized graphene structures are detailed here, and we show that the SAM architecture can be tailored for use in emerging applications, *e.g.*, electrically stimulated nerve fiber growth *via* the targeted binding of specific cell surface peptide sequences on the functionalized graphene scaffold. The simulations quantify the changes in film physisorption on graphene and alkyl chain packing efficiency as the film surface is made more polar by changing the terminal groups from methyl ($-\text{CH}_3$) to amine ($-\text{NH}_2$) to hydroxyl ($-\text{OH}$) groups. The mode of molecule packing dictates the orientation and spacing between terminal groups at the surface of the SAM, which determines the way in which successive layers build up on the surface, whether *via* formation of bilayers of the molecule or the immobilization of other (macro)molecules, *e.g.*, proteins, on the SAM. The simulations show formation of ordered, stable assemblies of monolayers and bilayers of decylamine-based molecules on graphene. These films can serve as protein adsorption platforms, with a hydrophobin protein showing strong and selective adsorption by binding *via* its hydrophobic patch to methyl-terminated films and binding to amine-terminated films using its more hydrophilic surface regions. Design rules obtained from modeling the atom-scale structure of the films and interfaces may provide inputs to experiments for rational design of assemblies in which the electronic, physicochemical and mechanical properties of the substrate, film and protein layer can be tuned to provide the desired functionality.

KEYWORDS: graphene functionalization, self-assembly, bilayers, alkylamine, hydrophobin protein, computer-aided design, molecular dynamics, nanostructured scaffolds, cell immobilization.

INTRODUCTION

The substrate-templated self-organization of organic molecules into two- and three-dimensional functional architectures provides new nanostructured materials for technological applications,¹ given the demonstrated film structural stability and integrity provided by strong molecule-substrate adhesion and tight packing between molecules.²⁻³ The importance of such “bottom up” processes lies in their capability to build uniform, ultra-small functional units and the possibility to exploit such structures at nano-, meso- and macro-scopic scale for life science and nanotechnology applications.⁴⁻⁵ Self-assembled monolayers (SAMs) provide recognition of specific molecules at the film surface for bio-sensing and tissue engineering applications,⁶⁻⁸ together with controlled charge transport through the films for electronics and (bio)nanotechnology applications.⁹⁻¹⁰ While SAM platforms potentially provide a direct means of setting macroscopic physical, chemical and biological properties by nano-scale engineering,¹¹⁻¹⁵ detailed multi-scale experiments and simulations are necessary to identify, quantify and then control the atom-scale interactions that drive their assembly.¹⁶⁻²³ In general, the assemblies are found to be stabilized by individually weak non-covalent interactions that, summed over large areas, provide tightly-woven and extensive self-assembled structures.²⁴⁻²⁶ Once assembled, these structures can serve as platforms for adsorption of materials such as biomolecules and nanoparticles.^{21, 27-29}

The purpose of the present work is to probe the role of SAM-substrate adsorption, intra-SAM molecule-molecule packing and SAM-protein binding in the assembly of SAM-based protein adsorption platforms, using atom-scale computer simulations, as sketched in Figure 1. Given the potential usefulness of architectures that combine graphene, SAM and protein components, we focus on modeling the formation of mono- and bi-layered films on graphene from alkylamine molecules terminated in methyl, amine and hydroxyl groups, and probe the protein recognition properties of the films by adsorbing hydrophobin proteins on the film surfaces. The resulting graphene-SAM-protein assemblies combine (a) the electronic and physicochemical properties of a graphene substrate^{3, 30-31} with (b) the

non-covalent adsorption properties, SAM packing ability and charge transport properties of alkylamine molecules^{29, 32} and (c) the selective hydrophobic and hydrophilic binding properties of electrically-conductive hydrophobin proteins.³³⁻³⁵

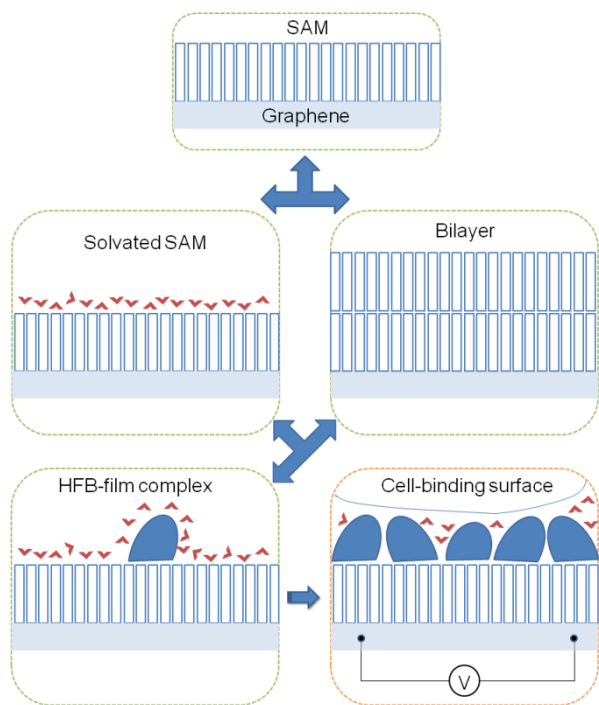


Figure 1. Schematic depicting the competing solvation, bilayer formation and protein adsorption effects in the self-assembly of a nanostructured platform on graphene that could potentially be used for electrically-stimulated tissue engineering, *e.g.*, to grow nerve cells. The assembly steps modeled in the present study as shown in green boxes. Future work towards engineering protein-cell surface recognition and electrical interfacing is sketched in the orange box.

The formation of alkylamine SAMs on various substrates including graphene²⁹ has been reported; *e.g.*, alkylamines SAMs on iron have been characterized using microscopy, spectroscopy, and molecular mechanics simulations.³⁶ Amine groups have also been shown to physisorb onto semiconducting carbon nanotubes,³⁷⁻³⁸ and n-type doping of nanotubes and graphene using ammonia or molecules containing amine groups has been reported by several groups.^{30, 39-40} Molecules including peptides and fluoroalkylsilanes have also recently been assembled into SAMs on graphene.⁴¹ Quantum mechanical and atomistic molecular dynamics simulations have aided the interpretation of experimental

1 data on molecule packing and SAM-substrate interface properties in these structures^{29, 36, 42} and have
2
3 also provided detailed mechanisms of self-assembly of various other graphene-molecule and graphene-
4
5 protein complexes; see, for example the recent simulation studies described in references⁴³⁻⁴⁷.
6
7

8
9 The simulations reported in the present work reveal the strong but terminal group-dependent
10 driving force for alkylamine chain packing on graphene. While the contributions of anchor, linker and
11 terminal groups to SAM formation are roughly additive, they are not independent; indicating that a
12
13 “modular” approach to nanostructured materials design requires modeling of the long-range architecture
14 to make reliable predictions about the film strength and function that may be obtained using different
15 molecules. Our results also highlight the tunable and protein-adhesive nature of the SAMs formed on
16 graphene, and further quantify the range of binding modes used by the hydrophobin protein on hydro-
17 phobic and hydrophilic surfaces.⁴⁸⁻⁵⁰ Once formed, the hydrophobin layer may provide an immobilized,
18 ordered protein scaffold for the recognition of specific cell surface peptide sequences, with the
19 underlying alkylamine molecules providing charge tunnelling paths to the bottom graphene layer, which
20 could be exploited for applications such as electrochemically stimulated growth of nerve fibers.⁵¹⁻⁵⁴
21
22

23 We use a comprehensive set of molecular simulations to address the question of whether or not
24 alkylamine-based SAMs can be engineered to serve as bio-immobilization platforms on graphene. The
25 simulation data allows us to make predictions concerning the usefulness of functionalized graphene
26 surfaces as platforms for immobilizing proteins (and cells), by quantifying: (a) SAM dynamics for
27 alkylamines with hydrophobic methyl terminal groups and more hydrophilic amine and alcohol
28 headgroups; (b) water solvation of SAMs; (c) assembly of molecular bilayers on graphene; (d) protein
29 adsorption on the graphene-based SAMs. Water, excess molecules and proteins compete for adsorption
30 on top of the SAMs, and the simulations allow us to estimate the populations of each type of alternative
31 solvated, bilayered and protein-bound regions on the SAM. The simulation data may thus provide some
32 preliminary design rules toward the realization of truly nanostructured platforms and scaffolds for
33
34

electro-stimulated tissue engineering, as well as for other applications including, *e.g.*, molecule-doped transparent graphene electrodes for solar cells and photoconductive “light-barrier” sensors.⁵⁵

RESULTS AND DISCUSSION

We first describe the atomic resolution molecular dynamics simulations of room temperature monolayer assemblies on graphene and then move to the simulations of bilayer formation and finally hydrophobin protein adsorption. The simulation results are discussed in relation to the state of the art in harnessing nanoscale structure, dynamics and energetics for the design of self-organizing, electrically-conductive interfaces.

Seventeen models were generated and subjected to extended, multi-nanosecond molecular dynamics simulations to model the formation of monolayers and bilayers (Figure 2), and monolayer-protein complexes on graphene. Models are listed in Table 1 and span three types of molecules, 1-aminodecane $\text{NH}_2(\text{CH}_2)_9\text{CH}_3$, 1,10-diaminodecane $\text{NH}_2(\text{CH}_2)_{10}\text{NH}_2$ and 10-amino-1-decanol $\text{NH}_2(\text{CH}_2)_{10}\text{OH}$, adsorbed on graphene in vacuum monolayer, water-solved monolayer, vacuum bilayer, and water-solvated monolayer-hydrophobin assemblies. More details on the models and simulation protocol are given in the Methods section. One of these seventeen models, the 1-aminodecane monolayer assembled on graphene under vacuum conditions, was previously reported in a joint experiment/simulation study of graphene non-covalent functionalization by alkylamines in a low dielectric solvent of 1:9 methanol:tetrahydrofuran.²⁹ While compatibility with aqueous environments is essential for interfacing the films with biomolecules, dry films are ideal for electrical measurements and so we calculate the properties of SAMs in water and in vacuum.

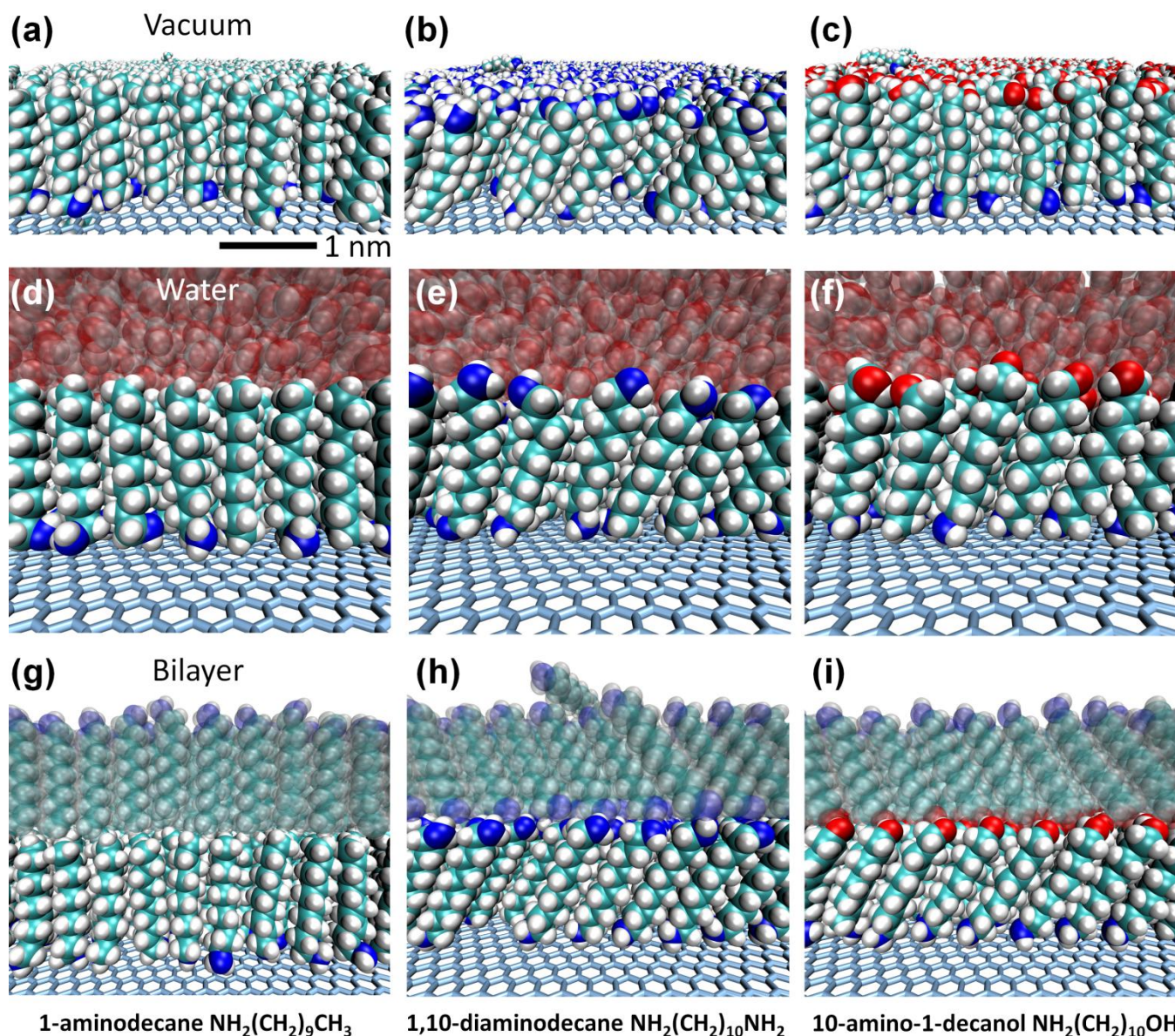


Figure 2. Computed film structures on graphene. Each subpanel shows a perspective view of typical molecule packing arrangements in film structures formed following room temperature molecular dynamics on a 13 nm x 15 nm graphene sheet. Methyl-, amine- and methanol-terminated SAMs are shown in panels (a), (b) and (c), respectively. Water-solvated SAMs and molecule bilayer structures are shown in panels (d)-(f) and (g)-(i). These final structures were computed following 12 ns of SAM dynamics and an additional 4 ns to model assembly of SAM/water interfaces or an additional 8 ns to model bilayer assembly *via* adsorption of a second layer of molecules on the SAM.

Table 1. List of graphene-bound film structures modeled in the current study.

Film	<i>Molecule type</i>			
	<i>1-amino decane</i>	<i>1,10-diamino decane</i>	<i>10-amino-1-decanol</i>	
	Number of atoms per cell			
SAM (12 ns)	33,856	35,424	34,640	
Solv. SAM (+4 ns)	230,920	231,702	230,930	
Bilayer (+8 ns)	60,512	63,648	62,080	
SAM-protein complex (+4 ns)	(a)	309,188	309,634	N/A
	(b)	309,212	309,682	N/A
	(c)	309,194	309,682	N/A
	(d)	309,209	309,592	N/A

The model size is expressed as number of atoms in each model; more details on cell contents, cell dimensions and simulation parameters are given in Methods. The three molecules are 1-aminodecane $\text{NH}_2(\text{CH}_2)_9\text{CH}_3$, 1,10-diaminodecane $\text{NH}_2(\text{CH}_2)_{10}\text{NH}_2$ and 10-amino-1-decanol $\text{NH}_2(\text{CH}_2)_{10}\text{OH}$. The post-equilibration sampling time for each model is given in parentheses next to each film type, and the “+” sign indicates the extra sampling performed on the final SAM structure to model SAM solvation and bilayer assembly. For the SAM-protein complexes, an additional 4 ns were performed starting from the final solvated SAM structure. Hydrophobin proteins were adsorbed in four different starting orientations, labeled (a)-(d) and described in the text. Protein adsorption was not computed on the $\text{NH}_2(\text{CH}_2)_{10}\text{OH}$ SAM, as this SAM shows a strong preference for forming NH_2 -terminated bilayers, as described in the text.

A. Molecular dynamics of alkylamine assembly on graphene

1) Computed SAM and bilayer structures: Figure 2 shows computed SAM structures on graphene. The SAMs form as a result of physisorption of the amine anchor groups of each molecule to graphene coupled with horizontal packing of the molecules into stable, upright monolayers. Second-order Møller–Plesset (MP2) perturbation theory calculations on a cluster model (methylamine on pyrene) yielded a binding energy of ~5 kcal/mol (1 kcal/mol ≈ 43.5 meV/molecule) for the amine-graphene interaction,²⁹ which is strong enough to enable formation of a stable aminodecane layer at room temperature.²⁹ The

binding was found to be mainly van der Waals in nature with only a small contribution from charge transfer, and the calculations found no strong preferential bonding site on the graphene plane.²⁹ Table 2 shows the computed self-assembly energies per molecule in each structure. As well as the SAM simulations in vacuum and in water, a third set of atomistic molecular dynamics simulations was performed. This third set of simulations measured the layering of excess molecules on top of the formed SAMs in order to understand how multi-layered structures assemble on graphene, which is important for applications of graphene as a platform in molecular device applications.⁵⁵

Table 2. Computed film self-assembly energies (kcal/mol) on graphene.

Film energy, kcal/mol		<i>Molecule type</i>		
		<i>1- amino decane</i>	<i>1,10- diamino decane</i>	<i>10- amino-1- decanol</i>
SAM	Elec	+0.6	-3.2	-3.7
	vdW	-21.1	-22.7	-20.5
	Total	-20.5	-25.9	-24.3
	(s.d.)	(0.5)	(0.6)	(1.6)
Water- solvated SAM	Elec	+6.3	-4.9	-5.4
	vdW	-23.3	-23.3	-22.4
	Total	-17.0	-28.2	-27.8
Bilayer	Elec	+0.8	-7.1	-9.7
	vdW	-20.1	-23.4	-22.1
	Total	-19.4	-30.5	-31.8
Solvation effect		+3.5 (1.9)	-2.3 (1.9)	-3.5 (2.0)
Bilayer effect		+0.9 (1.6)	+0.6 (1.8)	-1.6 (1.6)

Film self-assembly energies were computed from 200 structures sampled over the final 2 ns of room temperature molecular dynamics and are averaged over all molecules within the central 8 nm x 8 nm region of the film assembled on a 13 nm x 15 nm graphene sheet. Elec and vdW are electrostatic and van der Waals energies. A minus sign indicates structure stabilization. The number in parentheses below the Total energy is the time- and molecule-averaged uncertainty (s.d., standard deviation). Water-solvated SAM energies include the water-SAM interaction and the penalty for loss in water-water interactions (estimated as -5.3 kcal/mol from solvation at one face of a 8 nm x 8 nm monolayer of water molecules). Solvation of the bottom, unfunctionalized face of graphene is not included in the energy calculation. The “solvation effect” and “bilayer effect” calculations are explained in the text.

Table 2 shows that film assembly is dominated by van der Waals forces for the 1-aminodecane molecule, with electrostatics becoming significant as the polarity of the terminal group is increased. Electrostatic interactions account for 12% and 15% of the assembly energy in vacuum for the SAMs terminating in amine and hydroxyl groups respectively, and this electrostatic contribution rises slightly to 17% and 19% in the solvated SAMs and more sharply to 23% and 31% in the bilayer structures. As described below, the computed self-assembly energies may be rationalized on the basis of (non-covalent) bonding between terminal groups within a SAM layer, bonding between layers in a bilayer and competitive water interactions at the surface of the solvated SAMs (as sketched in Figure 1). As well as these direct, local interactions at the top of the SAM, the packing between the terminal groups also influences packing of the underlying alkyl chains and packing of amine anchor groups on the graphene substrate, meaning that the effect of terminal group “switching” is not confined to the top of the SAM.

The main prediction from the data in Table 2 is that only the most polar terminal group (-OH) will preferentially favor formation of molecule bilayers on graphene. While the “solvation effect” values given in Table 2 compare the stability of vacuum and solvated SAMs, the “bilayer effect” compares mono- and bi-layer assemblies, with details given in Supporting Information section S1 (Table S1 and Figure S1). The computed bilayer effect values in Table 2 predict populations of bilayered to solvated SAMs of approximately 15:1 for the amino alcohol. By contrast, SAMs are preferred for the less polar 1,10-diaminodecane and 1-aminodecane molecules, with estimated SAM: bilayer populations of 1:3 and 1:5, respectively.

Measured AFM height profiles for ordered regions of aminodecane films on graphene also showed monolayer formation.²⁹ As expected, the methyl-terminated molecule is most stable in vacuum, with a +3.5 kcal/mol penalty for water solvation due to the very low polarity of the -CH₃ group.⁵⁶ While earlier simulations showed that alkanethiol SAMs on gold contain low-density film defect regions that can adsorb excess molecules,²⁰ and also that SAMs damaged by AFM tips can adsorb water,⁵⁷ the

present, nearly defect-free SAMs and hydrophobic graphene substrate cause a net repulsive interaction with water for the methyl-terminated SAM (Table 2). The computed energies indicate that a low population of approximately 1:5 of bilayers to monolayers may be expected, slightly less than that predicted for the diamine molecule, with the inter-layer methyl-methyl contacts a poor substitute for amine anchoring to graphene. As shown in Table 3 below, the amine-graphene physisorption contact stabilizes the assembly by approximately -5 kcal/mol, which outweighs the approximately -2 kcal/mol benefit for solvation (Table 2, 1,10-diaminodecane SAM solvation effect) that could be obtained in a 1-aminodecane bilayer (Figure 2g and Figure S1).

Table 3 shows the computed contributions to the overall SAM self-assembly energies (Table 2), of amine anchor physisorption and packing, alkyl packing and terminal group packing, as well as contributions from solvation and bilayer formation. The computed energies in Table 3 show that the strength of physisorption on graphene of methyl-terminated and amine-terminated molecules through their amine anchor groups does not depend strongly on the assembly, whether SAM in vacuum, water-solvated SAM or bilayer of molecules. The most significant change in physisorption strength is for the alcohol with a -2.5 kcal/mol, or >50%, stronger physisorption in the bilayer structure. The structural analysis in the next section (section II) *Structural origin of the measured alkylamine-on-graphene self-assembly mechanisms* shows how reduced atom mobility (lower root mean square flexibilities, RMSF) contributes to the stronger film-graphene adhesion for the 10-amino-1-decanol bilayer, compared with 10-amino-1-decanol SAMs.

The similarity of methylamine packing energies (Table 3) for all molecules and for all structure types is striking and indicates that (a) the bottom amine groups pack closely on graphene irrespective of the molecule terminal group and more importantly (b) the amines pack identically when present at the surface of bilayer structures, where they become effectively the terminal groups at the surface of the bilayer (Figure 2). Neither graphene, water nor an extra top layer of molecules significantly affects

amine packing, with time-averaged differences of ≤ 0.8 kcal/mol computed from the data in Table 3, which are of the same order as the error estimates on individual values (standard deviations, Table 2).

Table 3. Computed components of film self-assembly energies (kcal/mol) on graphene.

Component kcal/mol	Terminal group	SAM	Solv. SAM	Bilayer la.1, la.2
Physisorp- tion	-CH ₃	-5.1	-5.1	-4.5, N/A
	-CH ₂ NH ₂	-5.5	-5.1	-5.4, N/A
	-CH ₂ OH	-4.4	-5.0	-6.9, N/A
-CH₂NH₂ anchor packing	-CH ₃	+9.4	+9.4	+9.4, +9.6
	-CH ₂ NH ₂	+10.0	+9.8	+9.7, +9.8
	-CH ₂ OH	+9.4	+9.8	+9.6, +9.7
(CH₂)₈ alkyl packing	-CH ₃	-24.5	-24.5	-24.5, -24.3
	-CH ₂ NH ₂	-40.3	-39.1	-40.7, -40.2
	-CH ₂ OH	-33.4	-33.6	-33.6, -33.5
Terminal group packing	-CH ₃	-0.3	-0.3	-0.3, -0.3
	-CH ₂ NH ₂	+10.0	+10.5	+9.7, +9.7
	-CH ₂ OH	+4.2	+7.2	+6.8, +6.8
Solvation/ Bilayer assembly	-CH ₃	N/A	+3.7	-1.9 (67% t.)
	-CH ₂ NH ₂	N/A	-4.3	-6.8 (74% t.)
	-CH ₂ OH	N/A	-6.1	-11.3 (76% t.)

Energies shown are physisorption, molecule packing and solvation/bilayer assembly components for the total film self-assembly energies which were given in Table 2 along with electrostatic and van der Waals contributions and error estimates. For the bilayer structure, values are given for layer1 and layer2 separated by a comma (la.1, la.2). Layer1 is the layer physisorbed directly to graphene. The bilayer assembly value is the interfacial energy between the layers and includes SAM desolvation penalties for the hydrophilic amine- and hydroxyl-terminated SAMs. The percentage in parentheses gives the contribution of the terminal groups to the inter-layer stabilization in the bilayer structures.

The amine packing values (Table 3) are positive, $\sim +10$ kcal/mol, due to unfavorable electrostatic $N^{\delta-} \cdots H^{\delta+}$ repulsion between cramped NH₂ groups, as the amines pack close enough to allow overall efficient molecule packing. The net full-molecule packing stabilization is achieved through alkyl chain contacts, in this case (CH₂)₈. This eight-carbon chain connects the -CH₂NH₂ anchor with the -CH₃, -CH₂NH₂ or -CH₂OH terminal groups, and packs efficiently in vacuum, solvated and bilayer structures. The time-averaged (CH₂)₈ chain packing energies are the same to within 0.2 kcal/mol (well below the inherent error in the averages, Table 2) in the methyl and alcohol terminated films, with a slight benefit

of approximately 1-2 kcal/mol obtained by reducing the number of competitive water interactions by forming bilayers (Figure 2 and Figure S1), which reduces the flexibility of the chains (Table 4). Taken together, the alkyl and terminal group packing data in Table 3 show how the overall assembly is optimized by amine physisorption coupled with tight methylene packing in the chains which drives the non-covalent functionalization of graphene by alkylamine molecules.²⁹

The stabilizing SAM-substrate physisorption and SAM chain packing interactions are partially balanced and offset by electrostatic penalties at either end of the molecule. These penalties are due to size mismatch between the endgroups and the alkyl chain, and indicate that the alkyl chain must be sufficiently long to direct formation of ordered, tightly-packed SAMs on graphene. This is in addition to the well-known requirement that the alkyl chain must be sufficiently long (and the surface concentration of molecules must be sufficiently high) to trigger formation of an upright SAM, as opposed to molecules physisorbed lengthways on graphene. Given that the amine molecules are physisorbed on graphene,²⁹ molecule-substrate covalent bond angles do not affect SAM packing. This contrasts with SAM formation of metals and metal oxides,⁵⁸ which is generally coupled with molecule chemisorption by formation of strong, directional bonds between the molecule anchor and substrate atoms. Finally, the tight surface coverage of molecules on graphene (5.6 ± 0.1 molecules/nm², averaged over all structures) and the regular spacing between molecules (see structural analysis in the next section) means that any bilayer formation is limited to a 2-D interface between layers, unlike the 3-D interfaces which are possible for more irregularly-packed SAMs formed on, *e.g.*, nanoparticles⁵⁹ and metal oxide surfaces,⁶⁰ which can feature, respectively, splayed chain conformations and irregularly-spaced substrate-molecule binding sites. These irregularly-packed SAMs can direct formation of porous SAMs that can be stabilized by interdigitation between molecules on opposing faces, which does not occur in the present physisorbed (but tightly-packed) alkylamine SAMs and bilayers on graphene.

II) Structural origin of the measured alkylamine-on-graphene self-assembly energies: The structural origin of these changes in film packing energies (due to changes in the magnitude of the cohesive van der Waals and electrostatic interactions between the molecules) may be understood by examination of local packing environments, molecule flexibilities and molecule tilts. These effects may be measured from the simulations by computing radial distribution functions around the anchor -NH_2 nitrogen atoms and around the terminal atoms (RDF, Figure 3), by calculating molecule root mean square fluctuations around the average positions of the atoms (RMSF values, Table 4) and computing the angle between the plane normal to the graphene and the plane of the anchor amine nitrogen atom and the outermost alkyl carbon atom (tilt angles, Table 4). These terminal atoms correspond to the -CH_3 carbon in the methyl-terminated SAM, the -NH_2 nitrogen in the amine-terminated SAM, and $\text{-CH}_2\text{OH}$ carbon and oxygen atoms in the hydroxyl-terminated SAM.

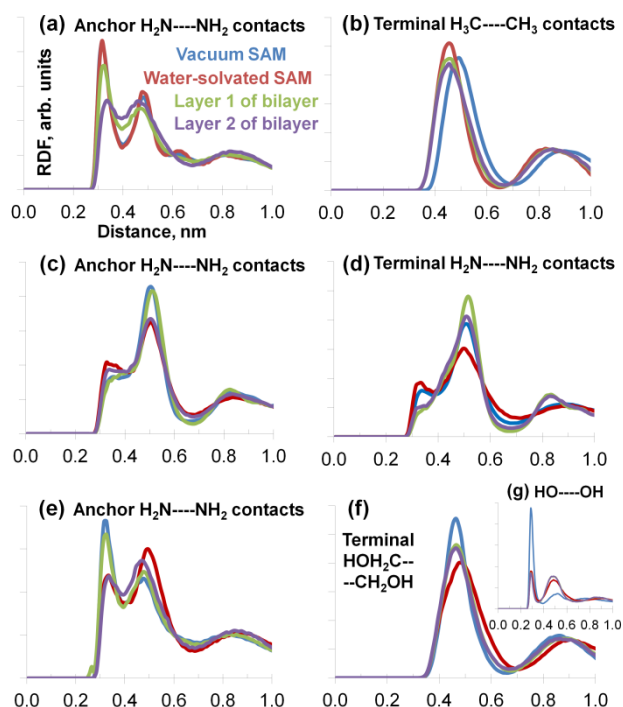


Figure 3. Radial distribution function, RDF, plots for the films assembled on graphene. Panels (a), (c) and (e) show contacts between nitrogen atoms in the amine anchor groups that physisorb on graphene, for (a) 1-aminodecane, (c) 1,10-diaminodecane and (e) 10-amino-1-decanol films. Panel (b) shows contacts between terminal carbon atoms in the 1-aminodecane films and panel (d) shows contacts between terminal nitrogen atoms in the 1,10-diaminodecane films. Panel (f) shows contacts between

terminal carbon atoms in the 10-amino-1-decanol films, with inset panel (g) showing contacts between the hydroxyl oxygen atoms.

The RDF plots in Figure 3 show that the $-\text{CH}_3$ terminal group packing in the 1-aminodecane film tightens slightly in the solvated SAM (Figure 3b) while the $-\text{NH}_2$ anchor group packing is loosened in the bilayer structure (Figure 3a). These effects are due to the repulsive interaction with water (Figure 3b) and loss in graphene-induced ordering in the bilayer, particularly in the top layer (Figure 3a). These structural perturbations are reflected also in the computed RMSF values (Table 4) with SAM molecule flexibility reduced in the solvated structure and increased in the bilayer. These structural effects are responsible for the calculated preference for a single, dry SAM of methyl-terminated alkylamine molecules on graphene, rather than solvated and bilayer structures (Table 2).

Table 4. Computed molecule flexibilities and tilt angles in SAM-functionalized graphene.

	<i>Terminal group</i>	SAM	Solv. SAM	Bilayer la.1, la.2
Molecule RMSF, Å	$-\text{CH}_3$	0.8	0.6	0.8, 1.1
	$-\text{CH}_2\text{NH}_2$	0.7	1.1	0.5, 0.7
	$-\text{CH}_2\text{OH}$	1.0	0.8	0.6, 0.7
$-\text{CH}_2\text{NH}_2$ anchor RMSF, Å	$-\text{CH}_3$	0.9	0.8	1.0, 1.3
	$-\text{CH}_2\text{NH}_2$	0.8	1.2	0.6, 0.8
	$-\text{CH}_2\text{OH}$	1.3	0.9	0.8, 0.9
$(\text{CH}_2)_8$ alkyl RMSF, Å	$-\text{CH}_3$	0.7	0.5	0.7, 1.0
	$-\text{CH}_2\text{NH}_2$	0.6	1.0	0.6, 0.8
	$-\text{CH}_2\text{OH}$	0.9	0.7	0.6, 0.7
Terminal group RMSF, Å	$-\text{CH}_3$	1.0	0.7	0.9, 1.2
	$-\text{CH}_2\text{NH}_2$	1.0	1.4	0.5, 0.6
	$-\text{CH}_2\text{OH}$	1.1	1.0	0.7, 0.7
Molecule tilt angle, °	$-\text{CH}_3$	6 ± 3	6 ± 5	$8 \pm 4, 8 \pm 7$
	$-\text{CH}_2\text{NH}_2$	36 ± 3	33 ± 5	$36 \pm 4, 35 \pm 7$
	$-\text{CH}_2\text{OH}$	8 ± 3	31 ± 5	$19 \pm 9, 17 \pm 13$

Root mean square fluctuation values (RMSF) have standard deviations ≤ 0.2 Å, with averages calculated over the same sampling region and structures used in the energy calculations (Tables 2-3). The molecule tilt angles are measured between the nitrogen of the amine anchor group and the terminal carbon atom, *i.e.*, the carbon of terminal group $-\text{CH}_3$, $-\text{CH}_2\text{NH}_2$ or $-\text{CH}_2\text{OH}$. Standard deviations in the tilt angles are given as \pm values after the time- and structure-averaged tilt angle.

On the other hand, for the di-amine film, the molecules are significantly more flexible when water is present on top of the film and the molecules are slightly less flexible in the bilayer (Table 4). These flexibilities reflect the changes in molecule packing arrangements in the solvated and bilayer environments, with a higher proportion of too-close, repulsive amine-amine contacts in the solvated SAM (panels (c) and (d) of Figure 3), while the opposite effect is present for the bilayer structures, with inter-layer amine-amine contacts ordering the molecules at the optimum amine packing distance.⁵⁶ The assembly energies in Table 2 indicate a mild net preference of -2.3 ± 1.9 kcal/mol for solvation of the amine-terminated film, mainly due to electrostatic stabilization of the polar $-\text{NH}_2$ groups at the film-water interface (Table 2 and Table 3). Solvation and bilayer formation on the amine-terminated SAM are near-isoenergetic (Table 2) with a very small computed difference of $+0.6 \pm 1.8$ kcal/mol in favor of solvation, due to mutually compensating electrostatic stabilization and van der Waals penalties for bilayer formation; comparing the RDF plots for the solvated and bilayer structures in panels (c) and (d) of Figure 3 shows that these competing electrostatic and van der Waals effects originate from the slightly looser amine packing in the bilayer.

Finally, the OH-terminated film shows significantly less molecule flexibility in both the solvated SAM and bilayer structures (Table 4). Thus, the very polar $-\text{OH}$ terminal groups change the SAM response to solvation and bilayer formation, compared with the moderately polar terminal $-\text{NH}_2$ groups. The RDF plots in Figure 3 show a reversed response to solvation for the alcohol compared with the di-amine molecule. Solvation, and to a lesser extent bilayer formation, decreases the repulsive amine anchor contacts. This is due to the very ordered H-bonding network that forms between the terminal alcohol groups and the top layer of water or alcohol molecules, which damps the motion of the molecules on the surface (Table 4) and gives a significant preference for solvated and bilayer structures (Table 2). While methyl-terminated and amine-terminated SAMs remain tilted (Table 4), by approximately 7° and 34° respectively, only the hydroxyl-terminated SAM shows an environmental

response, tilting from 8° to 31° upon solvation and from 8° to 18° upon bilayer formation (Table 4 and Figure 2). Chain tilt angles of $\sim 30^\circ$ are well known to stabilize methylene packing in alkyl SAMs on gold,² by optimising $C_n\cdots H_{n+1}$ contacts^{20, 60-61} to simultaneously minimize van der Waals and electrostatic potentials.⁵⁶ The more tilted orientations for amine- vs. methyl-terminated SAMs reflects the better matching of molecule anchor and terminal groups in the di-amine film, as discussed above and in Supporting Information section S2, and the improvement in chain tilts in the solvated and bilayered alcohol films is reflected in the computed stabilization energies (Table 2).

Overall, the computed stable, robust and virtually defect-free alkylamine film assembly on graphene is in excellent agreement with experiment²⁹ and points to useful applications of a range of different surface terminations in tuning the surface hydrophobicity of the films, to aid phase transfer of graphene between different environments (different solvents and solutions with different pH and ionic strengths) and to direct self-assembly of materials on top of the films. In the following section we take a further step in exploring self-assembly chemistry on functionalized graphene. We model adsorption of protein molecules on top of the SAMs, which may provide leads for experimental realization of functionalized graphene platforms for adsorption of biomolecules, towards the development of graphene-based molecular electronic and sensing devices.⁵⁵

B. Molecular dynamics of hydrophobin protein adsorption on monolayer-protected graphene

1) Computed protein-SAM structures: We now present protein-SAM structures on graphene calculated by modeling the adsorption of a hydrophobin (HFB) protein on top of the SAMs. We investigated four alternative starting protein orientations (Figure 4) on top of the 1-aminodecane and 1,10-diaminodecane SAM surfaces (Table 1), discounting (for the present study) the 10-amino-1-decanol SAM as it forms predominantly bilayers in conditions of excess 10-amino-1-decanol (Table 2) with amine groups

1 pointing outwards at the surface (Figure 2 and Figure S1) and so we approximate the film formed on
2 graphene by 10-amino-1-decanol molecules as the NH₂-terminated 1,10-diaminodecane SAM.
3
4

5
6 The structure of the HFB protein molecule is shown in Figure 4, which also highlights the
7 existence of the hydrophilic regions and hydrophobic patch region and so potential for controlled,
8 selective adhesion of hydrophobin on the SAM surface. Experiments and simulations show^{33, 35, 48, 50, 63,}
9
10
11
12
13
14
15
16
17
18
19
20
21
22
23
24
25
26
27
28
29
30
31
32
33
34
35
36
37
38
39
40
41
42
43
44
45
46
47
48
49
50
51
52
53
54
55
56
57
58
59
60
64 that it is possible to deposit the hydrophobins selectively on hydrophobic substrates including
graphene, which shows conductivity about 100 times greater than that of silicon and so could offer many
improvements to electroactive biological sensors and scaffolds.^{35, 65} Crucially for potential applications
in medical diagnostics and therapeutics (*e.g.*, electrically stimulated tissue repair/engineering) the
hydrophobin layer shows (a) very sharp resonances in current-voltage curves at room temperature⁶⁶ and
(b) can be engineered by attaching other proteins or metal nanoparticles for further functionalization.³⁵
Our results described below provide the atom-scale structure, dynamics and energetics of graphene-
SAM-hydrophobin interfaces, which may benefit efforts to exploit hydrophobin proteins in
nanostructured hybrid materials.⁶⁷ Surface ordering effects⁶⁸ and conformational changes in the protein (both
in native form and in engineered mutant forms)⁶⁹ will affect the electrical response and so influence the
ability of the protein to act as a charge conduit between the SAM surface and immobilized cells.

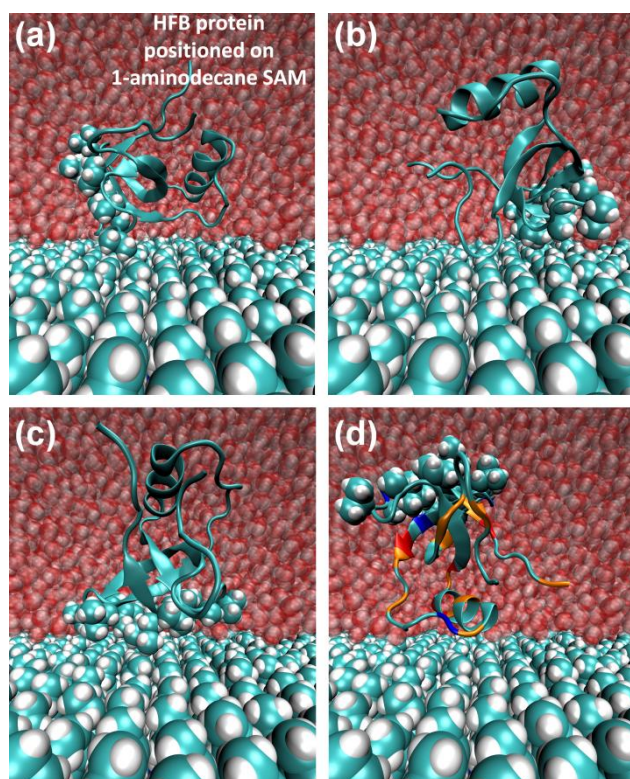


Figure 4. The four HFB protein starting orientations used to model protein adsorption on the SAM-functionalized graphene substrates. The film shown is the 1-aminodecane SAM; similar models were generated for the 1,10-diaminodecane SAM, as listed in Table 1. SAM atoms are shown as space-filling spheres, with the aqueous environment represented by transparent space-filling water atoms (with foreground waters removed for clarity). The protein contains about 100 amino acids, and the surface is mainly hydrophilic, but two β -hairpin loops contain several sidechains that form a flat “hydrophobic patch” that makes the molecule amphiphilic. The protein C α backbone is drawn in cartoon representation and the sidechain atoms of the hydrophobic patch residues are shown as space-filling spheres (identified in the X-ray structure⁶² by the large cluster of uncharged residues comprised of Val18, Leu19, Leu21, Ile22, Val24, Val54, Ala55, Val57, Ala58, Ala61, Leu62 and Leu63). In panel (d) the remaining residues are colored (in C α cartoon representation) by type: light blue – non-polar amino acids; orange – polar; blue – negatively charged; red – positively charged. Structures computed during 4 ns of equilibrated molecular dynamics are shown in Figure 5.

Computed protein adsorption energies are given in Table 5. Strong favorable van der Waals contacts drive the assembly of protein-SAM interfaces at the methyl-terminated surface, with orientation (c) (Table 5, Figure 4 and Figure 5) showing the strongest interaction. The small but consistently favorable contribution of electrostatic interactions reflects long-range stabilization of the weakly polar terminal $-\text{CH}_3$ groups by the four negatively-charged aspartate and four positively-charged lysine

residues that are positioned between 9 Å and 27 Å away from the protein-SAM interface in all four complexes; hydrophobin is a small protein with a relatively low proportion of charged residues.

Table 5. Computed protein-SAM adsorption energies on SAM-functionalized graphene.

Protein-SAM adsorption, kcal/mol	Terminal group	Electrostatic	van der Waals	Total
Orientation (a)	-CH ₃	-4.3 (2.4)	-24.5 (4.6)	-28.8 (6.2)
	-CH ₂ NH ₂	-12.3 (9.8)	-12.3 (3.8)	-24.6 (11.7)
Orientation (b)	-CH ₃	-4.5 (2.4)	-30.2 (5.5)	-34.8 (7.2)
	-CH ₂ NH ₂	-37.3 (19.7)	-12.2 (3.9)	-49.6 (20.0)
Orientation (c)	-CH ₃	-4.7 (1.5)	-42.3 (5.3)	-46.9 (5.9)
	-CH ₂ NH ₂	-3.5 (7.0)	-11.3 (3.1)	-14.8 (7.6)
Orientation (d)	-CH ₃	-1.2 (1.9)	-27.2 (4.8)	-28.4 (5.3)
	-CH ₂ NH ₂	-9.2 (9.3)	-11.8 (4.7)	-20.9 (10.2)

Adsorption energies were estimated from HFB-SAM van der Waals and electrostatic interaction energies. Error estimates are in parentheses and were averaged over 300 structures, sampling every 10 ps during the final 3 ns of dynamics.

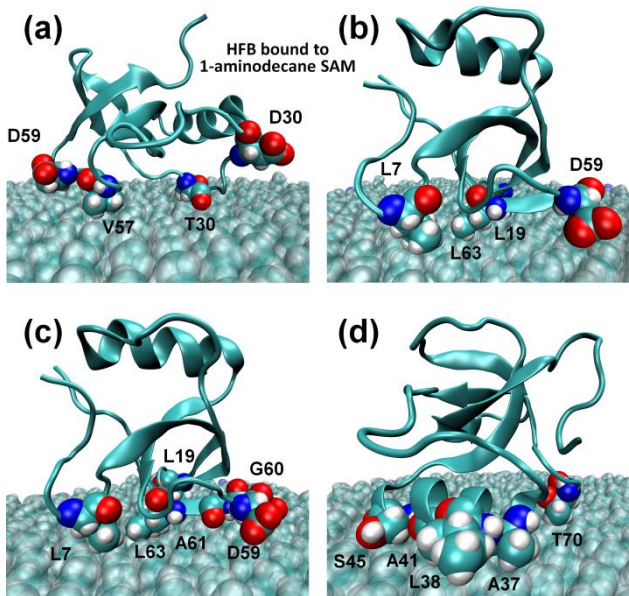


Figure 5. Representative protein-SAM-graphene complexes calculated during 4 ns of dynamics for the 1-aminodecane SAM. Similar atom representations are used as in Figure 4 above, with the exceptions that here all water molecules are omitted for clarity and protein residues making strong contributions to binding (see components in Figure 7 below) are labelled and shown in space-filling representation.

The four orientations provide a first approximation to an assembly mechanism on the 1-aminodecane surface in which proteins that land initially in an “upside down” orientation (d) rotate through orientations such as (a) and (b) to obtain the most stable orientation (c) in which the hydrophobic patch residues are orientated towards the surface. This orientation provides a tight seal between the protein and the film surface that reduces repulsive interactions with water for the HFB protein hydrophobic patch⁴⁸ and hydrophobic SAM surface methyl groups (Table 2). On the other hand, the amine-terminated surface of the 1,10-diaminodecane SAM on graphene forms a very strong complex to the protein in the simulation starting from orientation (b) (Figure 4). The high binding energy of -50 ± 20 kcal/mol (Table 5) is due to the interaction of charged residues Lys46, Asp25, Lys27 and Asp 59 with the amine terminal groups of the SAM. This strong protein-amine complex is shown in Figure 6a, with the two near-surface lysine residues forming strong, water-mediated H-bonds to the amine surface. Figure 6b shows an alternative, less stable complex, with an estimated binding energy of -21 ± 10 kcal/mol. This complex formed from starting orientation (d) (Figure 4) and is notable for the participation of a free 1,10-diaminodecane molecule in stabilizing the protein, principally through coordination with residue Lys49. Such highly mobile molecules are a ubiquitous feature of SAM interfaces.^{20, 61}

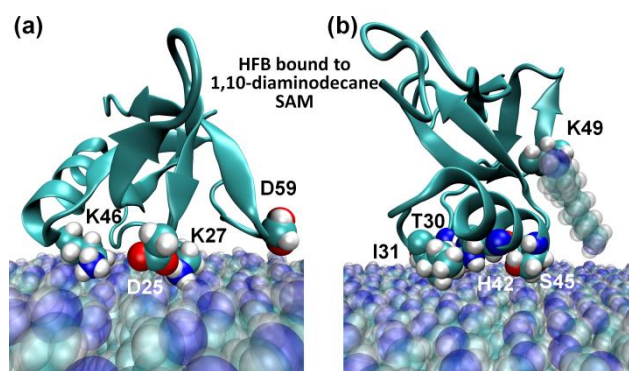


Figure 6. Representative protein-SAM-graphene complexes calculated during 4 ns of dynamics for the 1,10-diaminodecane SAM. (a) The strongest HFB-SAM complex, formed from starting orientation b (Figure 4 and Table 5); (b) A weak HFB-SAM complex that is stabilized by a free diaminodecane molecule in solution, formed from starting orientation d (Figure 4 and Table 5). Two additional weak HFB-SAM complexes (Table 5), not shown, were also formed in the simulations.

As shown by the computed energies in Table 5, the time averaged protein-SAM binding energies have higher standard deviations for the amine-terminated surface compared with the methyl-terminated surface. This is because water molecules mediate and bridge protein adsorption on the amine-terminated surface, giving complexes that are more flexible than those formed through the hydrophobic patch adsorption on the methyl-terminated SAM. The identification of strong binding energies between hydrophobin and the amine-terminated surface indicates the potential usefulness of this film in aqueous biotechnology applications including sensing and tissue engineering,⁵⁵ with a tight interface provided by electrostatic interactions between charged protein residues and the polar amine surface. Compared with the methyl-terminated surface, the selective adsorption of hydrophobin to surfaces on the basis of matching hydrophathy/polarity is clear, and in agreement with contemporaneous simulations of similar interfaces.⁵⁰

Note finally that the computed high likelihood of bilayer assembly on the 10-amino-1-decanol SAM (Table 2) means that we may expect an adsorbing protein to interact with an effectively amine-terminated solvated surface (Figure 2). This prediction applies to experimental conditions that use the excess molecule concentrations and molecule amine anchor groups modelled in the present study, with OH---OH inter-layer bonding calculated to be more favourable than NH₂-graphene physisorption (Table 3 and Figure S1). Hence simple rinsing of the film²⁹ may not be sufficient to remove these bilayers, but this remains to be tested experimentally. The computed self-assembly energies in Table 2 indicate that a 10-amino-1-decanol film will, we predict, form predominantly bilayers with amine groups pointing outwards at the surface (Figure 2i and Figure S1), and so exhibit protein adhesivity similar to that of the 1,10-diaminodecane film. Hence we do not further consider direct protein adsorption on the hydroxyl-terminated surface in the present work. However, this (potentially very useful, aqueous) interface is a subject of current calculations, and could be obtained experimentally by using conditions different to those modelled in the present study, *e.g.*, by using limiting (low) concentrations of molecules and/or

1 using molecules with alternative anchor groups that stick more strongly to graphene. For example,
2
3 alkanethiols have recently been predicted to have binding energies of 0.3 eV,⁷⁰ marginally higher than
4
5 the 0.2 eV binding calculated for alkylamines on pristine graphene.²⁹ Furthermore, thiol adsorption to
6
7 Stone-Wales defect sites (90° rotation of a carbon dimer) is predicted to have binding energies as high as
8
9 0.8 eV.²⁹ Hence, film assembly at defect sites, and along grain boundaries such as the pentagon-
10
11 heptagon pairs that stitch together grains in polycrystalline graphene,^{71, 72} could provide additional
12
13 functionalization strategies, as could film assembly on graphane and oxides of graphene.⁵⁵ It is also
14
15 possible that 10-amino-1-decanol molecules show a tendency to bind in “head-to-tail” orientations with
16
17 OH groups contacts to graphene, and this possibility is also currently being tested using quantum
18
19 mechanics and molecular dynamics simulations.
20
21
22
23
24
25
26
27

28 *II) Protein residues driving protein adsorption:* The computed protein residue components of the overall
29
30 protein adsorption energies (Table 5) on the methyl-terminated SAM are shown in Figure 7. For the
31
32 complex formed from starting orientation (a), the binding energy is made up of large, mutually-
33
34 compensating interactions from the Lys27-Asp59 salt bridge positioned ~8 Å away from the protein-
35
36 SAM interface, together with significant contributions from Asp34, Thr30 and Val57. For orientation
37
38 (b), the protein adsorption energy is due mainly to stabilizing interactions between the SAM surface
39
40 methyl groups and Asp59, Leu19, Leu63 and Leu7. In this orientation, Lys27 of the Lys27-Asp59 salt
41
42 bridge is rotated away to ~19 Å above the protein-SAM interface and so does not contribute directly to
43
44 interface formation.
45
46
47
48

49 Orientation (c) represents a more fully bound complex, with more residues participating in the
50
51 hydrophobic seal between the base of HFB and the methyl-terminated SAM. This complex has the
52
53 largest overall binding energy (Table 5) and the largest number of interface residues, with Asp59,
54
55 Leu63, Leu7, Leu19, Gln50, Ile22, Ala61 and Val54 all making a significant contribution to protein
56
57
58
59
60

adhesion on the SAM. While the negatively-charged Asp59 residue in the “hydrophobic patch” hinders HFB protein adsorption on non-polar surfaces (*e.g.*, bare Si(111)⁴⁸), the polarity of SAM molecules, even very weakly polar groups such as $-\text{CH}_3$, can use the electrostatic and van der Waals stabilization of the SAM terminal group by Asp59 to aid HFB adsorption.

Orientation (d), which is “upside down” compared with orientation (c), has the lowest calculated adsorption energy on the methyl-terminated SAM (Table 5). It also has the lowest number of stabilizing interface residues (Figure 7); Thr70 (the carboxy-terminus of the protein, see Figure 5), Ala41, Ala37, Ser45 and Ile38 stabilize this orientation, but it remains as weak as the alternative binding orientation that uses some a small subset of the hydrophobic patch residues (orientation a). This “upside down” orientation is also significantly weaker than orientations that use most (orientation b) or all (orientation c) of the hydrophobic patch residues. Overall, stronger binding energies are due to participation of more residues at the interface with the SAM, rather than rotation of the protein to bring one or a few very adhesive residues towards the SAM; this type of multivalent, collectively-strong binding of multiple, individually-weak ligands is used extensively in nature, and increasingly in nanotechnology, in the assembly of kinetically stable interfaces.^{21, 73}

For the amine-terminated SAM, the strongest interaction with HFB is through the charged residues Lys46, Asp25, Lys27 and Asp59 (Figure 6a). These residues show components of -16, +5, -21 and -6 kcal/mol, accounting for 75% of the overall -50 kcal/mol protein adsorption energy, with electrostatic interactions predominating and accounting for 88% of the overall summed contribution of -37 kcal/mol from these four charged residues.

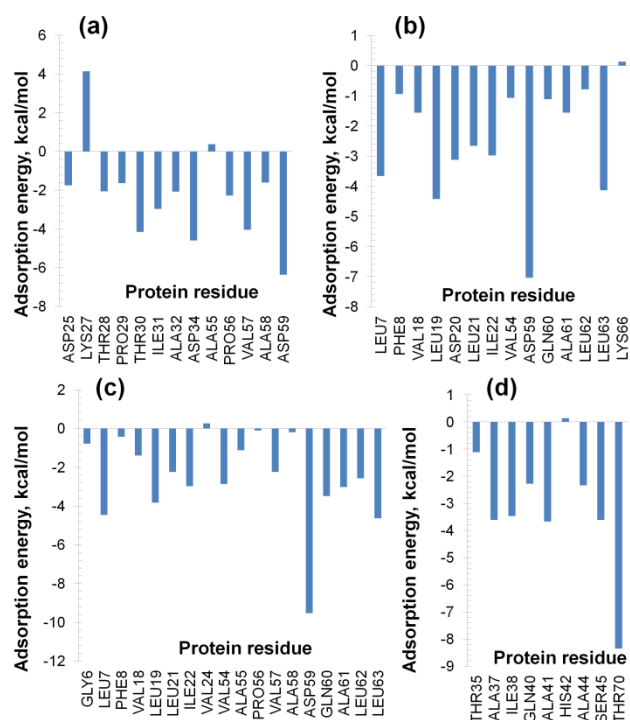


Figure 7. Computed contributions of individual protein residues to HFB protein adsorption on 1-aminodecane SAMs on graphene.

CONCLUSIONS

The present study describes the atom-scale mechanisms underlying self-assembly of alkylamine films on graphene and the role of film termination in stabilizing the adsorption of a model protein on the film. This hydrophobin protein can provide an electrically conductive interface between a secondary, more hydrophilic protein layer and the graphene substrate, which could ultimately be used to seed cells and electrically stimulate nerve tissue formation⁵¹⁻⁵⁴ on large area multi-protein hydrophobin films assembled on alkylamine-functionalized graphene. The hydrophobin adsorbs without significant denaturation on the surface of the films, with the alkyl groups linking the protein to graphene forming a tight, defect-free SAM for electronic coupling of the conductive protein with graphene. While bilayers can also form on graphene in the presence of a high local concentration of molecules per unit surface area of graphene, monolayers remain the predominant film type assembled using dodecanedecane molecules,²⁹ and the current simulations indicate a population of approximately 75% monolayers.

1
2 Bilayer formation is less favorable because the energy gain for assembly of the bilayer interface is offset
3
4 by the loss in solvation for the bottom layer and loss in graphene interactions for the top layer. While
5
6 monolayers also predominate for the monoamine molecule, the simulations predict that bilayer
7
8 formation becomes more favorable for 10-amino-1-decanol films on graphene, due to strong H-bonding
9
10 between layers.
11
12

13
14 By modeling adsorption of a hydrophobin protein on top of the solvated films, the simulations
15
16 show that the protein switches from using its basal “hydrophobic patch” to using more hydrophilic
17
18 surface residues for surface adsorption as the film surface is made more hydrophilic by changing the
19
20 terminal group from a methyl to an amine moiety. Crucially for mechanical (and electrical) interfacing
21
22 of graphene with the aqueous biological environment, the SAM packing remains highly ordered and
23
24 virtually defect free in water, and both the protein residues and film molecules at the interface form
25
26 strong contacts, resulting in a protein-film interface that competes with intra-protein residue-residue and
27
28 intra-film molecule-molecule contacts.
29
30
31

32
33 The main prediction from this modeling study is that alkylamine films can provide an ordered,
34
35 adhesive platform for protein immobilization. Future work will involve modeling the formation of multi-
36
37 protein films on functionalized graphene and investigating the cell adhesion properties of this protein
38
39 layer. As well as the hydrophobic adhesion of hydrophobin to a methyl-terminated surface, the results
40
41 obtained in the present work indicate that polar terminal groups can be used to make a tight interface
42
43 between the film and hydrophilic protein residues (*e.g.*, cell surface binding peptide motifs) that is
44
45 mediated by water molecules and which may be expected, for more hydrophilic proteins and over larger
46
47 areas, to form interfaces as strong as the multivalent, electrostatically-driven protein-protein interfaces
48
49 used to regulate biological processes. In addition, while many studies have used high level quantum
50
51 mechanical calculations to describe amine binding to inorganic substrates such as metals and metal
52
53 oxides (see, *e.g.*, references⁷⁴⁻⁷⁶), only a few studies have reported calculations of amine-graphene^{29, 77},
54
55
56
57
58
59
60

alkyl-protein⁷⁸ and direct protein-graphene^{77, 79-81} electronic interactions. Therefore, much computational work remains to be done to describe charge transfer from graphene to cell surface proteins *via* the SAM-hydrophobin interface, and will most likely require a combination of petascale computing, linear scaling density functional theory and/or well-parameterized semi-empirical methods. In the nearer term, deeper understanding of the atom-scale features of SAM assemblies on graphene, and the corresponding 3-D layering, will aid efforts to synthesize novel biomaterials in which the component building blocks and interfaces are engineered and arranged to provide structures tailored for specific device applications.

METHODS

The SAM models (Table 1 and Figure 2) feature a film of 784 molecules placed on a graphene sheet with surface area 13 nm x 15 nm, generating systems containing ~35,000 atoms. Graphene carbons were assigned neutral charges and constrained to their experimental positions throughout the simulations. Each film was relaxed using steepest descent minimization with respect to the CHARMM22 force field⁵⁶ and then brought to room temperature by gradually raising the temperature from 0 to 295 K over 2 nanoseconds of dynamics while simultaneously loosening positional constraints on the molecule non-hydrogen atoms. Each model was then subjected to 12 ns of free dynamics with no constraints on the film to allow formation of a well-equilibrated, stable structure. In all, 3 x 12 = 36 ns of production dynamics were performed for these monolayer assemblies using 1-aminodecane, 1,10-diaminodecane and 10-amino-1-decanol.

The final monolayer structures calculated following 12 nanoseconds of room temperature dynamics were used as starting structures for both water-solvated monolayer and vacuum bilayer models. Water solvation of each monolayer model was performed by encasing the model in a large 16 x 20 x 6 nm box of water molecules, producing ~231,000 atom cells which were minimized and thermalized using the same protocol as described above and then sampled for an additional 4 ns of room temperature dynamics each, 12 ns in all. Bilayer models were made by placing a second layer of molecules on top of the monolayer structures, and these ~62,000 atom cells were minimized and thermalized and then each of the three bilayers were subjected to a further 8 ns of room temperature dynamics, 24 ns in all. Finally, a hydrophobin protein was placed on top of the solvated monolayers in four different starting orientations (Figure 2), overlapping waters removed and extra waters added to

expand the water box size to 16 x 20 x 10 nm and ensure no spurious inter-cell protein-protein interactions, yielding model sizes of ~309,000 atoms. The formation of protein-film complexes (from four different starting protein orientations) was modeled for methyl and amine terminated films, for a further 4 ns of equilibrated room temperature dynamics, sampling for a total of $4 \times 4 \times 2 = 32$ ns. The full dataset comprised 104 ns of production dynamics for films and complexes assembled from each of the three molecules.

For the vacuum models, Ewald summation was used to calculate the electrostatic interactions by embedding the model in a large 18 nm x 18 nm x 12 nm vacuum box. For the solvated models, the cell sizes used corresponded to the dimensions of the water boxes. A 2 fs timestep was used for dynamics by constraining covalent bonds to hydrogen via the ShakeH algorithm.⁸² The distance between pairs of non-bonded atoms for inclusion in the pair list was set to 13.5 Å with a 12 Å cutoff and a switching function used between 10 and 12 Å. Langevin dynamics was used for non-hydrogen atoms with a damping coefficient of 5 ps⁻¹. The NAMD program⁸³ together with the CHARMM22 forcefield⁵⁶ was used for molecular dynamics with a NVT (constant number of particles, constant volume and constant temperature) ensemble for vacuum and NPT (constant number of particles, constant pressure and constant temperature) for solvated models. Image generation and Tcl script-based trajectory analysis was performed using the VMD program.⁸⁴

Acknowledgements. D.T. acknowledges Science Foundation Ireland (SFI) for financial support under Grant Number 11/SIRG/B2111 and computing resources at Tyndall and the SFI/Higher Education Authority Irish Centre for High-End Computing (ICHEC). C.A.N. thanks the Singapore National Research Foundation (NRF) for support through award number NRF-CRP 8-2011-07.

Supporting Information Available: Extraction of bilayer populations from computed assembly energies, comparison of alkylamine-on-graphene and alkanethiol-on-gold SAM structures, and control simulations of protein adsorption on bare non-functionalized graphene. This information is available free of charge *via* the Internet at <http://pubs.acs.org/>.

REFERENCES

1. Ariga, K.; Li, M.; Richards, G. J.; Hill, J. P. Nanoarchitectonics: A Conceptual Paradigm for Design and Synthesis of Dimension-Controlled Functional Nanomaterials. *J. Nanosci. Nanotechnol.* **2011**, *11*, 1-13.
2. Love, J. C.; Estroff, L. A.; Kriebel, J. K.; Nuzzo, R. G.; Whitesides, G. M. Self-assembled monolayers of thiolates on metals as a form of nanotechnology. *Chem. Rev.* **2005**, *105*, 1103-1169.
3. Wang, Q. H.; Hersam, M. C. Room-temperature molecular-resolution characterization of self-assembled organic monolayers on epitaxial graphene. *Nature Chem.* **2009**, *1*, 206-211.
4. Colombo, G.; Soto, P.; Gazit, E. Peptide self-assembly at the nanoscale: a challenging target for computational and experimental biotechnology. *Trends Biotechnol.* **2007**, *25*, 211-218.
5. Whitesides, G. M.; Lipomi, D. J. Soft nanotechnology: "structure" vs. "function". *Faraday Discuss.* **2009**, *143*, 373-384.
6. Motesharei, K.; Myles, D. C. Molecular recognition on functionalized self-assembled monolayers of alkanethiols on gold. *J. Am. Chem. Soc.* **1998**, *120*, 7328-7336.
7. Twardowski, M.; Nuzzo, R. G. Molecular recognition at model organic interfaces: Electrochemical discrimination using self-assembled monolayers (SAMs) modified via the fusion of phospholipid vesicles. *Langmuir* **2003**, *19*, 9781-9791.
8. Guo, Y.; Li, M. Y.; Mylonakis, A.; Han, J. J.; MacDiarmid, A. G.; Chen, X. S.; Lelkes, P. I.; Wei, Y. Electroactive oligoaniline-containing self-assembled monolayers for tissue engineering applications. *Biomacromolecules* **2007**, *8*, 3025-3034.
9. Qi, Y. B.; Ratera, I.; Park, J. Y.; Ashby, P. D.; Quek, S. Y.; Neaton, J. B.; Salmeron, M. Mechanical and charge transport properties of alkanethiol self-assembled monolayers on a Au(111) surface: The role of molecular tilt. *Langmuir* **2008**, *24*, 2219-2223.
10. Thuo, M. M.; Reus, W. F.; Nijhuis, C. A.; Barber, J. R.; Kim, C.; Schulz, M. D.; Whitesides, G. M. Odd-Even Effects in Charge Transport across Self-Assembled Monolayers. *J. Am. Chem. Soc.* **2011**, *133*, 2962-2975.
11. Aggeli, A.; Bell, M.; Boden, N.; Keen, J. N.; Knowles, P. F.; McLeish, T. C. B.; Pitkeathly, M.; Radford, S. E. Responsive gels formed by the spontaneous self-assembly of peptides into polymeric beta-sheet tapes. *Nature* **1997**, *386*, 259-262.
12. Terfort, A.; Bowden, N.; Whitesides, G. M. Three-dimensional self-assembly of millimetre-scale components. *Nature* **1997**, *386*, 162-164.
13. Lahann, J.; Mitragotri, S.; Tran, T. N.; Kaido, H.; Sundaram, J.; Choi, I. S.; Hoffer, S.; Somorjai, G. A.; Langer, R. A reversibly switching surface. *Science* **2003**, *299*, 371-374.
14. Yu, H. F.; Iyoda, T.; Ikeda, T. Photoinduced alignment of nanocylinders by supramolecular cooperative motions. *J. Am. Chem. Soc.* **2006**, *128*, 11010-11011.
15. Harada, A.; Kobayashi, R.; Takashima, Y.; Hashidzume, A.; Yamaguchi, H. Macroscopic self-assembly through molecular recognition. *Nature Chem.* **2011**, *3*, 34-37.
16. Lehn, J. M. Toward complex matter: Supramolecular chemistry and self-organization. *Proc. Natl. Acad. Sci. U. S. A.* **2002**, *99*, 4763-4768.
17. Raut, V. P.; Agashe, M. A.; Stuart, S. J.; Latour, R. A. Molecular dynamics simulations of peptide-surface interactions. *Langmuir* **2005**, *21*, 1629-1639.
18. Palmer, L. C.; Velichko, Y. S.; de la Cruz, M. O.; Stupp, S. I. Supramolecular self-assembly codes for functional structures. *Phil. Trans. R. Soc. A* **2007**, *365*, 1417-1433.
19. Nerngchamnon, N.; Li, Y.; Qi, D.; Jian, L.; Thompson, D.; Nijhuis, C. A. The role of van der Waals forces in the performance of molecular diodes. *Nat. Nanotech.* **2013**, DOI: 10.1038/NNANO.2012.238.
20. Gannon, G.; Greer, J. C.; Larsson, J. A.; Thompson, D. Molecular Dynamics Study of Naturally Occurring Defects in Self-Assembled Monolayer Formation. *ACS Nano* **2010**, *4*, 921-932.
21. Perl, A.; Gomez-Casado, A.; Thompson, D.; Dam, H. H.; Jonkheijm, P.; Reinhoudt, D. N.; Huskens, J. Gradient-driven motion of multivalent ligand molecules along a surface functionalized with multiple receptors. *Nature Chem.* **2011**, *3*, 317-322.
22. Zhao, J.; Wang, Q.; Liang, G.; Zheng, J. Molecular Dynamics Simulations of Low-Ordered Alzheimer beta-Amyloid Oligomers from Dimer to Hexamer on Self-Assembled Monolayers. *Langmuir* **2011**, *27*, 14876-14887.
23. Thompson, D.; Hermes, J. P.; Quinn, A. J.; Mayor, M. Scanning the Potential Energy Surface for Synthesis of Dendrimer-Wrapped Gold Clusters: Design Rules for True Single-Molecule Nanostructures. *ACS Nano* **2012**, *6*, 3007-3017.
24. Chandler, D. Interfaces and the driving force of hydrophobic assembly. *Nature* **2005**, *437*, 640-647.
25. Mann, S. Self-assembly and transformation of hybrid nano-objects and nanostructures under equilibrium and non-equilibrium conditions. *Nat. Mater.* **2009**, *8*, 781-792.
26. Rybtchinski, B. Adaptive Supramolecular Nanomaterials Based on Strong Noncovalent Interactions. *ACS Nano* **2011**, *5*, 6791-6818.
27. Sapsford, K. E.; Medintz, I. L.; Golden, J. P.; Deschamps, J. R.; Uyeda, H. T.; Mattoussi, H. Surface-immobilized self-assembled protein-based quantum dot nanoassemblies. *Langmuir* **2004**, *20*, 7720-7728.
28. Ludden, M. J. W.; Li, X.; Greve, J.; van Amerongen, A.; Escalante, M.; Subramaniam, V.; Reinhoudt, D. N.; Huskens, J. Assembly of bionanostructures onto beta-cyclodextrin molecular printboards for antibody recognition and lymphocyte cell counting. *J. Am. Chem. Soc.* **2008**, *130*, 6964-6973.
29. Long, B.; Manning, M.; Burke, M.; Szafrank, B. N.; Visimberga, G.; Thompson, D.; Greer, J. C.; Povey, I. M.; MacHale, J.; Lejosne, G.; Neumaier, D.; Quinn, A. J. Non-Covalent Functionalization of Graphene Using Self-Assembly of Alkane-Amines. *Adv. Funct. Mater.* **2012**, *22*, 717-725.
30. Novoselov, K. S.; Geim, A. K.; Morozov, S. V.; Jiang, D.; Zhang, Y.; Dubonos, S. V.; Grigorieva, I. V.; Firsov, A. A. Electric field effect in atomically thin carbon films. *Science* **2004**, *306*, 666-669.
31. Geim, A. K. Graphene: Status and Prospects. *Science* **2009**, *324*, 1530-1534.
32. McDermott, S.; George, C. B.; Fagas, G.; Greer, J. C.; Ratner, M. A. Tunnel Currents across Silane Diamines/Dithiols and Alkane Diamines/Dithiols: A Comparative Computational Study. *J. Phys. Chem. C* **2009**, *113*, 744-750.
33. Szilvay, G. R.; Paananen, A.; Laurikainen, K.; Vuorimaa, E.; Lemmetyinen, H.; Peltonen, J.; Linder, M. B. Self-assembled hydrophobic protein films at the air-water interface: Structural analysis and molecular engineering. *Biochemistry* **2007**, *46*, 2345-2354.
34. Wang, Z. F.; Lienemann, M.; Qiao, M.; Linder, M. B. Mechanisms of Protein Adhesion on Surface Films of Hydrophobin. *Langmuir* **2010**, *26*, 8491-8496.
35. Laaksonen, P.; Kainlahti, M.; Laaksonen, T.; Shchepetov, A.; Jiang, H.; Ahopelto, J.; Linder, M. B. Interfacial Engineering by Proteins: Exfoliation and Functionalization of Graphene by Hydrophobins. *Angew. Chem.-Int. Ed.* **2010**, *49*, 4946-4949.
36. Feng, Y. Y.; Chen, S. H.; You, J. M.; Guo, W. J. Investigation of alkylamine self-assembled films on iron electrodes by SEM, FT-IR, EIS and molecular simulations. *Electrochim. Acta* **2007**, *53*, 1743-1753.
37. Kong, J.; Dai, H. J. Full and modulated chemical gating of individual carbon nanotubes by organic amine compounds. *J. Phys. Chem. B* **2001**, *105*, 2890-2893.

38. Chattopadhyay, D.; Galeska, I.; Papadimitrakopoulos, F. Metal-assisted organization of shortened carbon nanotubes in monolayer and multilayer forest assemblies. *J. Am. Chem. Soc.* **2001**, *123*, 9451-9452.
39. Schedin, F.; Geim, A. K.; Morozov, S. V.; Hill, E. W.; Blake, P.; Katsnelson, M. I.; Novoselov, K. S. Detection of individual gas molecules adsorbed on graphene. *Nat. Mater.* **2007**, *6*, 652-655.
40. Wang, X. R.; Li, X. L.; Zhang, L.; Yoon, Y.; Weber, P. K.; Wang, H. L.; Guo, J.; Dai, H. J. N-Doping of Graphene Through Electrothermal Reactions with Ammonia. *Science* **2009**, *324*, 768-771.
41. Khatayevich, D.; So, C. R.; Hayamizu, Y.; Gresswell, C.; Sarikaya, M. Controlling the Surface Chemistry of Graphite by Engineered Self-Assembled Peptides. *Langmuir* **2012**, *28*, 8589-8593.
42. Yokota, K.; Takai, K.; Enoki, T. Carrier Control of Graphene Driven by the Proximity Effect of Functionalized Self-assembled Monolayers. *Nano Lett.* **2011**, *11*, 3669-3675.
43. Titov, A. V.; Kral, P.; Pearson, R. Sandwiched Graphene-Membrane Superstructures. *ACS Nano* **2010**, *4*, 229-234.
44. Ou, L. C.; Luo, Y.; Wei, G. H. Atomic-Level Study of Adsorption, Conformational Change, and Dimerization of an alpha-Helical Peptide at Graphene Surface. *J. Phys. Chem. B* **2011**, *115*, 9813-9822.
45. Cheng, C. L.; Zhao, G. J. Steered molecular dynamics simulation study on dynamic self-assembly of single-stranded DNA with double-walled carbon nanotube and graphene. *Nanoscale* **2012**, *4*, 2301-2305.
46. Yu, X.; Wang, Q. M.; Lin, Y. A.; Zhao, J.; Zhao, C.; Zheng, J. Structure, Orientation, and Surface Interaction of Alzheimer Amyloid-beta Peptides on the Graphite. *Langmuir* **2012**, *28*, 6595-6605.
47. Fedorov, M. V.; Lynden-Bell, R. M. Probing the neutral graphene-ionic liquid interface: insights from molecular dynamics simulations. *Phys. Chem. Chem. Phys.* **2012**, *14*, 2552-2556.
48. Moldovan, C.; Thompson, D. Molecular dynamics of the "hydrophobic patch" that immobilizes hydrophobin protein HFBII on silicon. *J. Molec. Model.* **2011**, *17*, 2227-2235.
49. Mereghetti, P.; Wade, R. C. Diffusion of hydrophobin proteins in solution and interactions with a graphite surface. *BMC Biophysics* **2011**, *4*.
50. Liu, Y. Z.; Wu, M.; Feng, X. Z.; Shao, X. G.; Cai, W. S. Adsorption Behavior of Hydrophobin Proteins on Polydimethylsiloxane Substrates. *J. Phys. Chem. B* **2012**, *116*, 12227-12234.
51. Wallace, G. G.; Chen, J.; Li, D.; Moulton, S. E.; Razal, J. M. Nanostructured carbon electrodes. *J. Mater. Chem.* **2010**, *20*, 3553-3562.
52. Hess, L. H.; Jansen, M.; Maybeck, V.; Hauf, M. V.; Seifert, M.; Stutzmann, M.; Sharp, I. D.; Offenhausser, A.; Garrido, J. A. Graphene Transistor Arrays for Recording Action Potentials from Electrogenic Cells. *Adv. Mater.* **2011**, *23*, 5045-5049.
53. Park, S. Y.; Park, J.; Sim, S. H.; Sung, M. G.; Kim, K. S.; Hong, B. H.; Hong, S. Enhanced Differentiation of Human Neural Stem Cells into Neurons on Graphene. *Adv. Mater.* **2011**, *23*, H263-H267.
54. Higgins, M. J.; Molino, P. J.; Yue, Z. L.; Wallace, G. G. Organic Conducting Polymer-Protein Interactions. *Chem. Mater.* **2012**, *24*, 828-839.
55. Georgakilas, V.; Otyepka, M.; Bourlinos, A.B.; Chandra, V.; Kim, N.; Kemp, K.C.; Hobza, P.; Zboril, R.; Kim, K.S. Functionalization of Graphene: Covalent and Non-Covalent Approaches, Derivatives and Applications. *Chem. Rev.* **2012**, *112*, 6156-6214.
56. MacKerell, A. D.; Bashford, D.; Bellott, M.; Dunbrack, R. L.; Evanseck, J. D.; Field, M. J.; Fischer, S.; Gao, J.; Guo, H.; Ha, S.; Joseph-McCarthy, D.; Kuchnir, L.; Kuczera, K.; Lau, F. T. K.; Mattos, C.; Michnick, S.; Ngo, T.; Nguyen, D. T.; Prodhom, B.; Reiher, W. E.; Roux, B.; Schlenkrich, M.; Smith, J. C.; Stote, R.; Straub, J.; Watanabe, M.; Wiorkiewicz-Kuczera, J.; Yin, D.; Karplus, M. All-atom empirical potential for molecular modeling and dynamics studies of proteins. *J. Phys. Chem. B* **1998**, *102*, 3586-3616.
57. Lane, J. M. D.; Chandross, M.; Lorenz, C. D.; Stevens, M. J.; Grest, G. S. Water penetration of damaged self-assembled monolayers. *Langmuir* **2008**, *24*, 5734-5739.
58. Love, J. C.; Wolfe, D. B.; Haasch, R.; Chabynyc, M. L.; Paul, K. E.; Whitesides, G. M.; Nuzzo, R. G. Formation and structure of self-assembled monolayers of alkanethiols on palladium. *J. Am. Chem. Soc.* **2003**, *125*, 2597-2609.
59. Wang, J. C.; Neogi, P.; Forciniti, D. On one-dimensional self-assembly of surfactant-coated nanoparticles. *J. Chem. Phys.* **2006**, *125*, 194717.
60. Gannon, G.; O'Dwyer, C.; Larsson, J. A.; Thompson, D. Interdigitating Organic Bilayers Direct the Short Inter layer Spacing in Hybrid Organic-Inorganic Layered Vanadium Oxide Nanostructures. *J. Phys. Chem. B* **2011**, *115*, 14518-14525.
61. Gannon, G.; Larsson, J. A.; Greer, J. C.; Thompson, D. Quantification of Ink Diffusion in Microcontact Printing with Self-Assembled Monolayers. *Langmuir* **2009**, *25*, 242-247.
62. Hakanpaa, J.; Paananen, A.; Askolin, S.; Nakari-Setälä, T.; Parkkinen, T.; Penttilä, M.; Linder, M. B.; Rouvinen, J. Atomic resolution structure of the HFBII hydrophobin, a self-assembling amphiphile. *J. Biol. Chem.* **2004**, *279*, 534-539.
63. Talbot, N. J. Fungal biology - Coming up for air and sporulation. *Nature* **1999**, *398*, 295-296.
64. Kisko, K.; Szilvay, G. R.; Vuorimaa, E.; Lemmetyinen, H.; Linder, M. B.; Torkkeli, M.; Serimaa, R. Self-assembled films of hydrophobin protein HFBIII from *Trichoderma reesei*. *J. Appl. Crystallogr.* **2007**, *40*, S355-S360.
65. Zhou, K.; Thouas, G.A.; Bernard, C.C.; Nisbet, D.R.; Finkelstein, D.I.; Li, D.; Forsythe, J.S., Method to impart electro- and biofunctionality to neural scaffolds using graphene-polyelectrolyte multilayers. *ACS Appl. Mat. Inter.* **2012**, *4*, 4524-4531.
66. Kivioja, J. M.; Kurppa, K.; Kainlahti, M.; Linder, M. B.; Ahopelto, J. Electrical transport through ordered self-assembled protein monolayer measured by constant force conductive atomic force microscopy. *Appl. Phys. Lett.* **2009**, *94*, 183901.
67. Gruner, L. J.; Ostermann, K.; Rodel, G. Layer Thickness of Hydrophobin Films Leads to Oscillation in Wettability. *Langmuir* **2012**, *28*, 6942-6949.
68. Richter, W.; Boeuf, S.; Throm, T.; Gutt, B.; Strunk, T.; Hoffmann, M.; Seebach, E.; Muhlberg, L.; Brocher, J.; Gotterbarm, T. Engineering hydrophobin DewA to generate surface coatings that enhance adhesion of human but not bacterial cells. *J. Tissue Eng. Regen. M.* **2012**, *6*, 428-428.
69. Linder, M. B. Hydrophobins: Proteins that self assemble at interfaces. *Curr. Opin. Colloid Interface Sci.* **2009**, *14*, 356-363.
70. Qin, X.; Meng, Q.; Zhao, W. Interactions of Ethanethiol with Defective Graphene: First-Principle Calculations. *2010 Int. Conf. Nanotech. Biosens. IPCBEE*, **2011**, *2*, 80-84.
71. Huang, P.Y.; Ruiz-Vargas, C.S.; van der Zande, A.M.; Whitney, W.S.; Levendorf, M.P.; Kevek, J.W.; Garg, S.; Alden, J.S.; Hustedt, C.J.; Zhu, Y.; Park, J.P.; McEuen, P.L.; Muller, D.A. Grains and grain boundaries in single-layer graphene atomic patchwork quilts. *Nature* **2011**, *469*, 389-392.
72. Wei, Y.; Wu, J.; Yin, H.; Shi, X.; Yang, R.; Dresselhaus, M. The nature of strength enhancement and weakening by pentagon-heptagon defects in graphene. *Nat. Mater.* **2012**, *11*, 759-763.
73. Huskens, J. Multivalent interactions at interfaces. *Curr. Opin. Chem. Biol.* **2006**, *10*, 537-543.
74. Di Felice, R.; Corni, S. Simulation of Peptide-Surface Recognition. *J. Phys. Chem. Lett.* **2011**, *2*, 1510-1519.
75. Kokh, D. B.; Corni, S.; Winn, P. J.; Hoefling, M.; Gottschalk, K. E.; Wade, R. C. ProMetCS: An Atomistic Force Field for Modeling Protein-Metal Surface Interactions in a Continuum Aqueous Solvent. *J. Chem. Theory Comput.* **2010**, *6*, 1753-1768.
76. Almora-Barrios, N.; Austen, K. F.; de Leeuw, N. H. Density Functional Theory Study of the Binding of Glycine, Proline, and Hydroxyproline to the Hydroxyapatite (0001) and (0110) Surfaces. *Langmuir* **2009**, *25*, 5018-5025.

77. Smeu, M.; Zahid, F.; Ji, W.; Guo, H.; Jaidann, M.; Abou-Rachid, H. Energetic Molecules Encapsulated Inside Carbon Nanotubes and between Graphene Layers: DFT Calculations. *J. Phys. Chem. C* **2011**, *115*, 10985-10989.
78. Sun, Y.; Latour, R. A. Comparison of implicit solvent models for the simulation of protein-surface interactions. *J. Comput. Chem.* **2006**, *27*, 1908-1922.
79. Cazorla, C. Ab initio study of the binding of collagen amino acids to graphene and A-doped (A = H, Ca) graphene. *Thin Solid Films* **2010**, *518*, 6951-6961.
80. Ding, N.; Lu, X. Q.; Wu, C. M. L. Nitrated tyrosine adsorption on metal-doped graphene: A DFT study. *Comp. Mat. Sci.*, **2012**, *51*, 141-145.
81. Rajesh, C.; Majumder, C.; Mizuseki, H.; Kawazoe, Y. A theoretical study on the interaction of aromatic amino acids with graphene and single walled carbon nanotube. *J. Chem. Phys.* **2009**, *130*, 124911.
82. Ryckaert, J. P.; Ciccotti, G.; Berendsen, H. J. C. Numerical-integration of cartesian equations of motion of a system with constraints - molecular-dynamics of n-alkanes. *J. Comput. Phys.* **1977**, *23*, 327-341.
83. Phillips, J. C.; Braun, R.; Wang, W.; Gumbart, J.; Tajkhorshid, E.; Villa, E.; Chipot, C.; Skeel, R. D.; Kale, L.; Schulten, K. Scalable molecular dynamics with NAMD. *J. Comput. Chem.* **2005**, *26*, 1781-1802.
84. Humphrey, W.; Dalke, A.; Schulten, K. VMD: Visual molecular dynamics. *J. Molec. Graph.* **1996**, *14*, 33-38.

Table of Contents (TOC) Graphical Abstract

